

<b>Titre:</b> Title:	Reinforcing epoxy nanocomposites with functionalized carbon nanotubes via biotin–streptavidin interactions
<b>Auteurs:</b> Authors:	Rouhollah Dermanaki Farahani, Hamid Dalir, Vincent Le Borgne, Loick A. Gautier, My Ali El Khakani, Martin Lévesque et Daniel Therriault
<b>Date:</b>	2012
<b>Type:</b>	Article de revue / Journal article
<b>Référence:</b> Citation:	Farahani, R. D., Dalir, H., Le Borgne, V., Gautier, L. A., El Khakani, M. A., Lévesque, M. & Therriault, D. (2012). Reinforcing epoxy nanocomposites with functionalized carbon nanotubes via biotin–streptavidin interactions. <i>Composites Science and Technology</i> , 72(12), p. 1387-1395. doi: <a href="https://doi.org/10.1016/j.compscitech.2012.05.010">10.1016/j.compscitech.2012.05.010</a>



### Document en libre accès dans PolyPublie

Open Access document in PolyPublie

<b>URL de PolyPublie:</b> PolyPublie URL:	<a href="https://publications.polymtl.ca/10401/">https://publications.polymtl.ca/10401/</a>
<b>Version:</b>	Version finale avant publication / Accepted version Révisé par les pairs / Refereed
<b>Conditions d'utilisation:</b> Terms of Use:	CC BY-NC-ND



### Document publié chez l'éditeur officiel

Document issued by the official publisher

<b>Titre de la revue:</b> Journal Title:	Composites Science and Technology (vol. 72, no 12)
<b>Maison d'édition:</b> Publisher:	Elsevier
<b>URL officiel:</b> Official URL:	<a href="https://doi.org/10.1016/j.compscitech.2012.05.010">https://doi.org/10.1016/j.compscitech.2012.05.010</a>
<b>Mention légale:</b> Legal notice:	

**Ce fichier a été téléchargé à partir de PolyPublie,  
le dépôt institutionnel de Polytechnique Montréal**

This file has been downloaded from PolyPublie, the  
institutional repository of Polytechnique Montréal

<http://publications.polymtl.ca>

# 1 **Reinforcing epoxy nanocomposites with functionalized carbon** 2 **nanotubes via biotin-streptavidin interactions**

3  
4 Rouhollah Dermanaki Farahani<sup>a</sup>, Hamid Dalir<sup>a</sup>, Vincent Le Borgne<sup>b</sup>, Loick. A. Gautier<sup>b</sup>, My Ali El  
5 Khakani<sup>b</sup>, Martin Lévesque<sup>a</sup>, and Daniel Therriault<sup>a\*</sup>

6 <sup>a</sup>Laboratory of Multiscale Mechanics, Center for applied research on polymers (CREPEC), École  
7 Polytechnique de Montreal, C.P. 6079, succ. Centre-Ville, Montreal (QC), H3C 3A7 (Canada)

8 <sup>b</sup>Institut National de la Recherche Scientifique, INRS-Énergie, Matériaux et Télécommunications,  
9 1650 Blvd. Lionel-Boulet, Varennes (QC), J3X 1S2 (Canada)

10 \* Corresponding author:

11 Phone: 1-514-340-4711 x4419; Fax: 1-514-340-4176;

12 E-mail: [daniel.therriault@polymtl.ca](mailto:daniel.therriault@polymtl.ca)  
13

## 14 **Abstract**

15 We report on the preparation of nanocomposites consisting of biofunctionalized single-walled  
16 carbon nanotubes (BF-SWCNTs) reinforcing an ultraviolet curable epoxy polymer by means of  
17 biotin-streptavidin interactions. The as-produced laser ablation SWCNTs are biofunctionalized  
18 via acid oxidization based purification process and non-covalent functionalization using  
19 surfactant, followed by grafting the resulting nanotubes with biomolecules. The biotin-grafted  
20 nanotubes are capable of interacting with epoxy groups in presence of streptavidin molecules by  
21 which chemical bridges between BF-SWCNTs and epoxy matrix are formed. The biomolecules  
22 grafted to the nanotubes surface not only facilitate the load transfer, but also improve the  
23 nanotube dispersion into the epoxy matrix, as observed by optical imaging and scanning  
24 electron microscopy. Mechanical characterization on the nanocomposite microfibers  
25 demonstrates considerable enhancement in both strength (by 76%) and modulus (by 93%) with  
26 the addition of only 1 wt.% of BF-SWCNTs. The electrical measurements reveal a clear change  
27 in electrical conductivity of nanocomposite microfibers reinforced with 1 wt.% of BF-SWCNTs  
28 in comparison to the microfibers containing solely purified carbon nanotubes. These  
29 multifunctional nanocomposite materials could be used to fabricate macro and microstructures

1 for a wide variety of applications such as high strength polymer nanocomposite and potential  
2 easily-manipulated biosensors.

3 **Keywords:** A. Carbon nanotube, surface modification, A. Nanocomposite, UV-assisted direct-write  
4

## 5 **1. Introduction**

6 Nanomaterials, such as single-walled carbon nanotubes (SWCNTs), are increasingly used to  
7 achieve multifunctional capabilities where they serve as an effective structural reinforcement, as  
8 well as large-surface platform for sensing purposes [1,2]. Owing to their high mechanical[3] and  
9 electrical [4] properties, SWCNTs show a strong potential for reinforcing polymers for a wide  
10 variety of applications such as high-performance structural composites [5,6], electromechanical  
11 actuators and sensors[7], non-destructive life prediction technology and shape memory  
12 polymers [8]. When compared to other polymer nanocomposites, nanotube-reinforced epoxy  
13 systems could exhibit high strength and multifunctional features for aircrafts and electronic  
14 products [6,9]. However, several fundamental challenges still have to be addressed in order to  
15 take full advantage of the excellent properties of the nanotubes. In particular, the ability to  
16 manipulate these entangled structures with their structurally smooth surface is required for their  
17 effective use in the development of nanodevices based on an individual nanotube or bulk  
18 nanotubes [10,11], as well as nanotube-reinforced nanocomposites [12-16].

19 The chemical treatment of carbon nanotubes surface significantly extends their potential for  
20 various applications. The surface functionalization of carbon nanotubes not only leads to their  
21 debundling, but also enables the design of an efficient interface to bond them to other active  
22 groups, like epoxy groups in nanocomposite materials. In particular, the purification induced  
23 covalent grafting of carboxylic groups at the surface of the nanotubes[17] as well as their non-  
24 covalent functionalization using surfactants like porphyrins[18] can be used to improve the  
25 reinforcing effect when compared to as-produced nanotubes. However, nanotube reinforcement

1 is still far from achieving its theoretical potential and new advances are needed for an efficient  
2 load transfer.

3 Functionalized nanotubes have been used for the immobilization of various biomolecules for  
4 biosensor applications [10]. Biomolecules bonded to functionalized nanotubes through  
5 functional groups are capable of interacting with other active biomolecules via reversible  
6 chemical bonding. Among these biomolecules, biotin-streptavidin bonding is known as one of  
7 the strongest interactions in nature [19,20]. Therefore, biotin-functionalized nanotubes could be  
8 used as a support to immobilize streptavidin molecules in biosensor applications. However,  
9 until now, most of the researches undertaken on using nanotubes in microelectronics have been  
10 limited to the use of an individual nanotube or bulk nanotubes. Due to the size order of an  
11 individual nanotube or their bulk physical state (i.e., powder of entangled structures),  
12 manufacturing and manipulation of these materials is quite challenging [10,11]. To address  
13 these difficulties, nanotubes have been added to a solution or a polymer matrix, suitable for use  
14 in electrospinning [21] and direct-write techniques [22]. Since fibers fabricated by  
15 electrospinning need additional patterning processes, the ultraviolet (UV)-assisted direct-write  
16 assembly [23] could be an alternative to manufacture complex microstructures with desired  
17 patterns when an UV-curable epoxy resin is used as a matrix.

18 Here, we report on the use of biotin-streptavidin interactions for further development of a  
19 multifunctional nanotube/epoxy composite system. This nanocomposite material was used for  
20 the fabrication of nanocomposite microfibers as an example of patterned microstructures for  
21 potential micro electromechanical systems (MEMS). Figure 1 shows the schematic of the  
22 fabrication process of nanocomposite microfibers suspended between two rectangular pads of  
23 nanocomposite by means of UV-assisted direct-write technique. To fabricate the  
24 nanocomposites, the SWCNTs were biofunctionalized via acidic treatment and non-covalent  
25 functionalization using surfactant, followed by grafting of biomolecules to chemically bridge

1 SWCNTs and epoxy matrix. The different steps of nanotubes functionalization were assessed  
2 using various structural characterization techniques. Finally, the effects of SWCNTs  
3 biofunctionalization and their dispersion on mechanical and electrical properties of the  
4 fabricated epoxy nanocomposite microfibers were studied to understand the nanocomposite  
5 structure-property relationship.

## 6 7 **2. Experimental details**

### 8 **2.1. SWCNTs synthesis, purification and biofunctionalization**

9 Single-walled carbon nanotubes were synthesized by using UV-laser ablation (248 nm, 20 ns,  
10 400 mJ) of a Co/Ni-doped (1.2 at. %) graphite target pellet. The KrF-laser ablation was  
11 performed under a controlled argon atmosphere at a temperature of 1150°C through a 45° quartz  
12 window (more experimental details on the KrF-laser synthesis and effects of key growth  
13 parameters can be found elsewhere [24,25]). The as-produced SWCNTs condensed on a water-  
14 cooled collector, located outside of the hot zone of the furnace, onto which they formed a thick  
15 rubbery-like film. This SWCNTs mat was peeled off and subjected to subsequent chemical  
16 purification treatment. The chemical purification treatment consisted of three main successive  
17 steps, each of which is targeted a specific purification. First, the Soxhlet extraction in toluene  
18 (for 1h) was conducted on the as-produced SWCNTs to remove residual fullerenes and some  
19 disordered carbon nanostructures in the deposit. Second, the SWCNTs were treated by hydrogen  
20 peroxide (10%) at room temperature (for 24 h) in order to crack the graphitic shells surrounding  
21 the residual catalyst nanoparticles. Finally, HNO<sub>3</sub> (3M) oxidation was conducted to remove  
22 metal catalyst particles and covalently functionalize the SWCNTs by the attachment of  
23 carboxylic groups at their surface. These chemically P-SWCNTs were collected by vacuum  
24 filtration on alumina filters (pore size 20 nm) and after successive rinsing cycles.

1 The desired amounts of P-SWCNTs and 1,3-diaminopropane 99% (D23602, Sigma-Aldrich),  
2 with a proportion of 1g P-SWCNTs/5 mL 1,3-diaminopropane 99%, were added to a solution of  
3 0.1 mM of zinc protoporphyrin IX (ZnPP, Sigma-Aldrich) in methanol. The suspension was  
4 sonicated in an ultrasonic bath (Ultrasonic cleaner 8891, Cole-Parmer) for 1 h. After  
5 ultrasonication, the mixture was shaken using a mixer/shaker (Spex CertiPrep 8000M  
6 Mixer/Mill) for 12 h at room temperature. The Soxhlet extraction for 2 h with methanol was  
7 performed on the aminated P-SWCNTs to remove any unreacted amine. The aminated P-  
8 SWCNTs were then added into a solution of 30 mL methanol containing desired amounts of  
9 biotin and N,N'-diisopropylcarbodiimide 99% (DIC, D125407, Sigma-Aldrich) with a  
10 proportion of 1g biotin/5 mL DIC. Biotinylation of the aminated P-SWCNTs were subsequently  
11 performed by shaking the resulting mixture using the mixer/shaker for 12 h at room  
12 temperature. Finally, these biotinylated nanotubes were washed with methanol twice, followed  
13 by rinsing with distilled water several times to remove any unreacted biotin.

14

## 15 **2.2. SWCNTs characterization**

16 The KrF-laser synthesized SWCNTs were systematically characterized by various techniques  
17 before and after their chemical purification and functionalization. Their Raman spectra were  
18 acquired at room temperature in the 100 - 2000  $\text{cm}^{-1}$  spectral region under ambient conditions  
19 using a back-scattering geometry on a microRaman microscope (Renishaw Imaging Microscope  
20 Wire TM) with a 50 $\times$  objective. A 514.5 nm (2.41 eV) line from an air cooled Ar<sup>+</sup> laser was  
21 used for excitation radiation. The chemical bonding states of the SWCNTs (before and after  
22 chemical purification) were analyzed by means of X-ray photoelectron spectroscopy (XPS)  
23 using the Cu K $\alpha$  monochromatic radiation (1486.6 eV) of an ESCALAB 200I-XL  
24 spectrophotometer. The purified, aminated and biotinylated SWCNTs were characterized by  
25 FT-IR (Digilab FTS7000) in order to characterize the chemical components attached to the

1 surface of the nanotubes and assess the biofunctionalization procedure. Finally, the  
2 nanostructural characteristics of as-produced, P-SWCNTs and BF-SWCNTs were directly  
3 examined by transmission electron microscopy (TEM) using a Jeol JEM-2100F (FEG-TEM,  
4 200 kV) microscope.

### 6 **2.3. Nanocomposite preparation**

7 The nanocomposite materials were prepared by mixing an Ultraviolet curable epoxy (UV-  
8 epoxy, UVE, UV15DC80, Master Bond Inc.) and either P-SWCNTs or BF-SWCNTs (at two  
9 loads of 0.5 wt.% and 1 wt.%). The UV-epoxy used in this study was a special one-component  
10 dual cure (ultraviolet/heat curable) epoxy resin which contains a UV photo-initiator having a  
11 maximum absorption at 365 nm and a heat-initiator active in the 60 – 80°C range. Biotin and  
12 1,3-diaminopropane 99% (1g biotin/5 mL 1,3-diaminopropane 99%) were stored in 30 mL  
13 acetone and ultrasonicated for 30 min. The desired amount of functionalized nanotubes was  
14 subsequently added to the solution. Then, the UV-epoxy was slowly mixed with the resulting  
15 solution over a magnetic stirring hot plate (Model SP131825, Barnstead international) at 50°C  
16 for 4 h. Finally, the streptavidin solution (1 mL 10 µg/mL, S4762, from streptomyces avidinii,  
17 Sigma-Aldrich) was slowly added to the nanocomposite mixture and stirred for 1 h. After  
18 stirring, the nanocomposite mixture was simultaneously sonicated and heated in the  
19 ultrasonication bath at 50°C for 2 h. The residual trace of solvent was evaporated by heating the  
20 nanocomposite mixture at 30°C for 12 h and at 50°C for 24 h in a vacuumed-oven (RK-52402,  
21 Cole Parmer). The biotin-streptavidin interaction is not affected by the temperature during the  
22 solvent evaporation process, since very specific and harsh conditions are required to break the  
23 strong biotin-streptavidin bond [19,20].

24 After evaporation of the solvent, the nanocomposites were passed through a very small gap in  
25 a three-roll mill mixer (Exakt 80E, Exakt Technologies) for final high shear mixing [26]. The

1 gaps between the rolls varied in three batch-wise progressing steps (10 passes each) with three  
2 different gaps at 25  $\mu\text{m}$ , 10  $\mu\text{m}$  and 5  $\mu\text{m}$ , respectively. The speed of the apron roll was adjusted  
3 to 250 RPM. The final mixture was then degassed under vacuum for 12 h. For comparison  
4 purposes, the nanocomposites with P-SWCNTs were also prepared using the same mixing  
5 procedure.

#### 7 **2.4. Nanocomposite morphological characterization**

8 For optical imaging purposes,  $\sim 20$   $\mu\text{m}$ -thick films of the nanocomposites were fabricated by  
9 direct deposition on a glass substrate by means of a computer-controlled robot (I & J2200-4, I &  
10 J Fisnar) that moves a dispensing apparatus (HP-7X, EFD) along the  $x$ ,  $y$  and  $z$  axes [22,27]. The  
11 quality of the mixing was observed for the cured nanocomposite films using an optical  
12 microscope (BX-61, Olympus) and image analysis software (Image-Pro Plus V5, Media  
13 Cybernetics). Microtomed surface of the bulk nanocomposite samples were also observed using  
14 field emission scanning electron microscopy (FESEM JEOL, JSM-7600TFE) in order to  
15 observe the nanotube dispersion.

#### 17 **2.5. Nanocomposite electrical and mechanical characterizations**

18 The ultraviolet-assisted direct-write technique [23] was used to fabricate nanocomposites  
19 microfibers in order to assess the reinforcing effects of P-SWCNTs and BF-SWCNTs in the  
20 epoxy matrix. Two parallel thick square pads of the nanocomposites with 6 mm gap were first  
21 fabricated by extruding the nanocomposites suspensions through a micro-nozzle (5127-0.25-B,  
22 Precision Stainless Steel Tips, EFD, internal diameter ( $ID$ ) = 150  $\mu\text{m}$ ) over a glass substrate.  
23 Right after, the pads were in situ cured using the optical fibers collected the light from two high-  
24 intensity UV light-emitting diodes (LED, NCSU033A, Nichia). Three suspended microfibers  
25 were then fabricated between two pads made of the same material. The microfibers were cured  
26 using UV exposure while being extruded (Figure 1). The electrical properties of the

1 nanocomposite microfibers were characterized using a Keithley 4200 semiconductor parametric  
2 analyzer with silver electrodes sputtered on the pads. Mechanical properties (tensile modulus,  
3 strength and elongation at break) of the nanocomposites microfibers were measured in a  
4 dynamic mechanical analyzer (DMA, DMA2980, TA instruments) using a film tension clamp.  
5 The microfibers were tested with a constant loading rate adjusted to reach failure within  $20 \pm 3$  s  
6 according to the ASTM D2256 standard. A minimum of five specimens from each  
7 nanocomposite sample were tested.

8

### 9 **3. Results and Discussion**

#### 10 **3.1. Nanotube structural characterization**

11 Figure 2(a) shows typical Raman spectra of the KrF-laser synthesized SWCNTs before and  
12 after their chemical purification. The peaks located in the  $100\text{-}300\text{ cm}^{-1}$  and the  $1500\text{-}1600\text{ cm}^{-1}$   
13 ranges are typical fingerprints of SWCNTs. The first peak is due to the radial breathing mode  
14 (RBM) of the SWCNTs while the second is associated with the tangential vibrations of the C  
15 atoms forming the nanotube surface (G band). The RBM peak centred around  $182\text{ cm}^{-1}$  arises  
16 from SWCNTs with a diameter of 1.26 nm [28]. The D band ( $1340\text{ cm}^{-1}$ ) is generally attributed  
17 to the presence of amorphous carbon (a-C) and/or disordered carbon (d-C). The G/D ratio is  
18 generally used to qualify the degree of purity of the nanotubes. Here, the G/D ratio is found to  
19 decrease for the purified SWCNTs (P-SWCNTs). This is in fact a consequence of the creation of  
20 defects on SWCNTs' surface by the nitric acid oxidation step in the purification process. This is  
21 further supported by XPS measurements shown in Figure 2(b). The main C 1s core level peak  
22 that arises from the C=C bonds is narrow in both samples at 284.5 keV. However, for P-  
23 SWCNTs, a shoulder appearing at 288 keV is also present in the spectrum. This component is  
24 attributed to the C-O-O carboxylic groups resulting from the covalent functionalization of the

1 nanotubes by the nitric acid treatment [29]. Based on the XPS results, it is fair to assume that  
2 the purification process led to carboxylic groups grafting onto the SWCNTs surfaces.

3 Figure 2(c) shows a typical TEM micrograph of the as-produced SWCNTs where the  
4 nanotubes are found to self assemble, most often into bundles with a diameter in the 5-20 nm  
5 range and lengths reaching up to few microns. Other structures, such as carbon-surrounded  
6 catalyst nanoparticles and/or graphitic nanostructures (i.e., dark spots in the micrograph) are  
7 also present. The various steps of purification are intended to remove residual metal catalyst  
8 nanoparticles and most of the undesired carbon forms (e.g., a-C, d-C, fullerenes). Figure 2(d)  
9 shows a typical TEM image of the P-SWCNTs. Nevertheless, one can still notice the presence  
10 of few dark spots that line the bundles. These are likely some residual catalyst nanoparticles,  
11 which were not entirely digested during the nitric acid oxidation treatment. Thermogravimetry  
12 analysis (TGA) measurements (not shown here) have demonstrated a substantial decrease (by  
13 more than 60%) in the concentration of residual catalyst in the P-SWCNTs samples, when  
14 compared to the as-produced SWCNTs.

15 FT-IR spectroscopy was also used to characterize the chemical components attached to the  
16 surface of SWCNTs. Figure 3(a) shows the FT-IR spectra of the functionalized SWCNTs at  
17 each step of the biofunctionalization process. The FT-IR spectrum of P-SWCNTs shows two  
18 specific bands at  $1315\text{ cm}^{-1}$  and  $1732\text{ cm}^{-1}$ , associated with carboxylic groups [30]. The  
19 aminated and biotinylated SWCNTs revealed an appearance of two new strong bands centered  
20 at  $1450\text{ cm}^{-1}$  and  $1479\text{ cm}^{-1}$ , confirming reactions between carboxylic and amino groups [31].  
21 The FT-IR spectrum of biofunctionalized carbon nanotubes (i.e., biotinylated SWCNTs) shows  
22 appearance of two new broad peaks centered around at  $1594\text{ cm}^{-1}$  and  $1635\text{ cm}^{-1}$ , which are  
23 assigned to  $2^\circ$  amide I and amide II, respectively [31]. The original amide groups of biotin as  
24 well as the amide bonds formed between amino groups on the aminated SWCNTs and  
25 carboxylic groups on the biotin are believed to be responsible for the two new peaks. The

1 appearance of these peaks in the spectrum of biofunctionalized SWCNTs (BF-SWCNTs) proves  
2 the grafting of the active biotin groups on the nanotubes surfaces through covalent bonds [31]. A  
3 high resolution TEM image (Figure 3(b)) shows individual P-SWCNTs with a very clean  
4 surface. This figure permits the direct measurement of the nanotube diameters (1.1-1.3 nm).  
5 Finally, Figure 3(c) shows a high-resolution TEM image of a SWCNT covered with a rough-  
6 looking material, most likely biomolecules or a mixture of carbonaceous residue and  
7 biomolecules, suggesting the effective presence of the grafted biomolecules on the SWCNTs  
8 surface [13].

### 10 **3.2. Morphology characterization**

11 Figures 4(a) and 4(b) show optical micrographs of two representative nanocomposites films  
12 with 1 wt.% loading of P-SWCNTs and BF-SWCNTs, respectively. The observed dark spots are  
13 thought to be nanotubes aggregates or nanotubes entangled around other carbonaceous  
14 materials. For the P-SWCNTs (Figure 4(a)), the majority of the nanotube aggregates are in the  
15 sub-micron range but some micron-size aggregates with a diameter of up to  $\sim 1\mu\text{m}$  are also  
16 present. A drastic change of the size of the aggregates was observed for the nanocomposite film  
17 with the BF-SWCNTs (Figure 4(b)). The larger spots observed for the P-SWCNTs-reinforced  
18 nanocomposite film became smaller, to  $0.7\mu\text{m}$  diameter (in average) when the BF-SWCNTs  
19 were used. To further support the optical observations, the cross-section of the nanocomposites  
20 microfibers was also observed under scanning electron microscopy (SEM). Figures 4(c) and  
21 4(d) show typical SEM images of the surface of nanocomposites with 1 wt.% loading of P-  
22 SWCNTs and BF-SWCNTs, respectively. In the purified SWCNT-reinforced nanocomposite,  
23 the nanotubes formed clusters and large aggregates (i.e., the bright spots). When the  
24 biofunctionalized SWCNTs were used, the large aggregates disappeared and it was difficult to  
25 spot clusters of SWCNTs. Based on all the above observations, the fairly uniform dispersion of

1 the nanotubes and their associated aggregates for both cases might be attributed to the  
2 effectiveness of the nanocomposite mixing procedure combining ultrasonication and three-roll  
3 mill mixing methods. Comparing the nanocomposites dispersion suggests that the presence of  
4 biomolecules at the nanotube-matrix interface prevented re-aggregation of nanotubes and  
5 improved the SWCNTs dispersion.

### 6 7 **3.3. Mechanical properties**

8 The effect of biofunctionalization of SWCNTs on the mechanical properties was assessed by  
9 tensile testing. Figure 5 shows the stress-strain curves along with their resulting histograms of  
10 the neat UV-curable epoxy (UV-epoxy) and its associated nanotube-reinforced nanocomposites,  
11 prepared either with the P-SWCNTs or BF-SWCNTs. Figure 5(a) shows an optical image of  
12 typical microfibers used in the tensile experiments and Figure 5(b) is a representative SEM  
13 image of a fiber cross-section after its fracture under tensile loading. The error bars on the  
14 histograms were calculated from the 95% confidence intervals on the mean value obtained from  
15 the measurements. When the BF-SWCNTs were added to the composite with 0.5 wt.% loading,  
16 the average modulus showed an increase of 59% compared to that of the neat resin and an  
17 increase of 19% when compared to that of the nanocomposite reinforced with the same  
18 nanotube loading of P-SWCNTs. The improvement of modulus for the composites with 1 wt.%  
19 BF-SWCNTs loading were found to be 93% and 16% when compared to those of the neat resin  
20 and the P-SWCNTs-reinforced composites, respectively. The increased stiffness, from the neat  
21 epoxy resin to the nanocomposites, might be attributed to the proper dispersion as well as  
22 beneficial orientation of the nanotubes that may occur during the extrusion of the  
23 nanocomposite through the micronozzle [32]. For both nanotube loadings, BF-SWCNTs led to  
24 nanocomposites ~20% stiffer than that obtained with P-SWCNTs. The contribution of possible  
25 orientation in this higher stiffness is unlikely, since all nanocomposite microfibers were

1 fabricated under the same extrusion conditions. Therefore, the further improvement of stiffness  
2 for the BF-SWCNT-based nanocomposites is most likely attributed to the increased effective  
3 aspect ratio of the BF-SWCNTs as a consequence of their better dispersion.

4 The average failure strength of the P-SWCNTs- and BF-SWCNTs-reinforced nanocomposite  
5 was also improved with the addition of nanotubes. The incorporation of 0.5 wt.% BF-SWCNTs  
6 to the epoxy matrix increased its strength by approximately 50%. The nanocomposite with 1  
7 wt.% BF-SWCNTs showed further enhancement (by 75%). For both nanotube loadings, higher  
8 failure strength (up to 24%) was achieved for the composites reinforced with BF-SWCNTs  
9 when compared to the P-SWCNTs-reinforced composites. More interestingly, the strength of  
10 the nanocomposite microfibers containing 0.5 wt.% BF-SWCNTs was found to be very close to  
11 that of the 1 wt.% P-SWCNTs-reinforced nanocomposite microfibers. This relatively higher  
12 improvement could be attributed to a possible strong nanotube/matrix interfacial interaction and  
13 to a good dispersion of nanotubes with the presence of the biomolecules. Considering the  
14 quantity of the SWCNTs added, these improvements of both modulus and strength are among  
15 the highest improvements for epoxy composites reported so far, as compared in Table 1  
16 [9,12,13].

#### 18 **3.4. Governing interaction mechanisms**

19 The possible governing interaction mechanisms between nanotubes and epoxy matrix with the  
20 presence of biomolecules are schematized in Figure 6. The proposed mechanism can be  
21 interpreted in the light of the mechanisms proposed by Wang et al. [31] and Sun et al. [12]. The  
22 nanotube biofunctionalization begins with grafting (covalently and non-covalently) carboxylic  
23 and amine groups to the surface of SWCNTs (more details on the synthesis procedure are found  
24 in experimental section). Grafting biomolecules on the nanotubes surface relies on the  
25 carboxylic groups created during the nanotube purification and on the use of Zinc

1 protoporphyrin IX (ZnPP) molecules. ZnPP molecules can non-covalently interact with the  
2 nanotubes wall through  $\pi$ - $\pi$  interactions [18,22]. It should be mentioned that the  
3 functionalization procedure used in this study is non-destructive to the sidewall by attaching  
4 functional groups to the nanotubes. Since the long acidic treatment can destroy the wall integrity  
5 and consequently affect the mechanical properties of the resulting nanocomposite, the duration  
6 of acidic treatment was effectively controlled in our purification process. The carboxylic groups  
7 are capable of interacting with the amine groups and could contribute to further grafting of  
8 biomolecules to the surface of nanotubes. Streptavidin molecules offer four active sites which  
9 are equally capable of binding with biotin. The streptavidin was added to the BF-SWCNTs  
10 mixture in the presence of epoxy resin in order to avoid possible consumption of their four  
11 active sites by BF-SWCNTs, since they should be still-active to bridge between BF-SWCNTs  
12 and epoxy matrix (Figure 6b). The proposed interaction mechanism between streptavidin, biotin  
13 and epoxy resin on the right side of Figure 6b (i.e., epoxy side) was inspired from the work done  
14 by Wang et al. [31]. Therefore, a very strong nanotube-epoxy cross-linked network could be  
15 obtained by the action of active streptavidin that binds to other biotin molecules, which are  
16 attached to either epoxy groups or BF-SWCNTs.

17 The formation of such chemical bonding is believed to be responsible for the reasonable  
18 increase of failure strength obtained for the BF-SWCNTs-reinforced nanocomposites. It is worth  
19 noting that the average failure strain of 1 wt.% BF-SWCNTs-reinforced nanocomposite  
20 microfibers showed a slight increase (by 19%) in comparison to that of neat epoxy microfibers.  
21 Considering the flexibility of SWCNTs and their highly elastic behavior, the improvement of  
22 failure strain might be another proof of strong interfacial interaction [9]. Another contribution  
23 might come from stretching the curved and entangled nanotubes during the mechanical  
24 solicitation [9]. These factors could contribute to the increased failure elongation only when the  
25 nanotubes are well-bonded to the matrix through strong interfacial interactions. Therefore, the

1 BF-SWCNTs could be used not only as a strong reinforcement but also to slightly improve  
2 failure strain and thus to increase toughening properties and impact resistance of intrinsically  
3 brittle epoxies as reported in the literature [9,12]. The toughening effect of the nanotubes might  
4 be further evolved from the non-linear response of the nanocomposites under strain [32], since  
5 the response of the neat epoxy resin is linearly elastic (Figure 5c). It has been reported that  
6 carbon nanotubes could promote effective toughening mechanisms such as crack bridging and  
7 shear banding, although these reasons were not experimentally verified here. When compared to  
8 current toughening methods such as rubber modification of epoxy resins which may decrease  
9 their other mechanical properties, well-bonded carbon nanotubes confer an extra benefit without  
10 sacrificing other properties. This benefit can be translated to epoxy-based traditional structural  
11 composites in order to improve the epoxy matrix toughness of composite laminates in which  
12 nanotubes are added to the epoxy matrix. Thus, the toughening affect might be the most  
13 important advantage of nanomodification in this new class of composites which are known as  
14 multiscale composites.

15

### 16 **3.5. Electrical conductivity**

17 The effect of biofunctionalization of the nanotubes on electrical conductivity was studied. The  
18 electrical conductivity of the P-SWCNTs and BF-SWCNTs-reinforced composite microfibers  
19 was characterized upon voltage application between two silver-coated pads. Figure 7 shows the  
20 measured current with respect to applied voltage (I-V) curve of the nanocomposite microfibers  
21 for two different nanotubes loadings. Linear responses, with different slopes ( $R$ ), of the currents  
22 versus the applied voltage were observed for all nanocomposite microfibers. For the microfibers  
23 with nanotube loading of 0.5 wt.%, the BF-SWCNTs were found to lead to slightly lower  
24 conductivities (by 19%), but this remains within the uncertainty of the measurements. At  
25 nanotube loading of 1 wt.%, the nanocomposite microfibers with BF-SWCNTs showed a

1 decrease of 129% in electrical conductance (i.e.,  $I/R$ ) when compared to that of P-SWCNTs-  
2 reinforced nanocomposite. The decrease of electrical conductivity might be attributed to the  
3 presence of streptavidin molecules that possibly act as a less-conductive layer surrounding the  
4 SWCNTs. The measured resistivity was decreased with the addition of more nanotubes (1 wt.%)  
5 through which more electrical percolation pathways should be formed. This could be described  
6 by the electrical conductivity mechanisms for the nanocomposites which are direct contact of  
7 nanotubes in their percolation pathways and/or electron tunneling between neighboring  
8 nanotubes at sufficiently close proximity [33]. Depending on nanotube loading, the contribution  
9 of these two mechanisms in the measured electrical conductivity varies. At the nanotube  
10 loading of 0.5 wt.%, electrons must travel through larger amounts of insulating epoxy matrix  
11 between the conductive nanotubes and the contribution of electron tunneling in the electrical  
12 conductivity is likely larger when compared to that of nanocomposites with 1 wt.% nanotubes.  
13 When more percolation conducting pathways are formed (at higher nanotube loadings),  
14 electrons conduct predominantly along the conductive nanotube pathways and thus, the effect of  
15 electron tunneling decreases [33]. For bio-functionalized nanotubes, the biomolecules might be  
16 placed between conductive nanotubes in their percolation pathways and affect the  
17 nanocomposite conductivity. Therefore, it is thought that the presence of biomolecules is more  
18 significant at higher nanotube concentrations and responsible for a clear change in the electrical  
19 conductivity of the nanocomposite microfibers containing 1 wt.% of SWCNTs. This  
20 phenomenon has been used for potential biosensor applications where streptavidin molecules  
21 are detected by their attachment to the surface of biotin-functionalized nanotubes [31,34].

22

#### 23 **4. Conclusions**

24 The surface biofunctionalization of SWCNTs and the utilization of an efficient mixing  
25 procedure enabled the full integration of nanotubes within an epoxy matrix. Although the

1 nanotube dispersion and mechanical properties of the nanocomposite reinforced with P-  
2 SWCNTs were reasonably improved in comparison to the neat epoxy, subsequent grafting of  
3 biotin molecules to the P-SWCNTs led to a fairly good dispersion and further enhancement in  
4 their reinforcing effect. The failure strength of nanocomposite microfibers reinforced with 1  
5 wt.% of BF-SWCNTs showed an increase of 76% when compared to that of pure resin and an  
6 increase of 25% when compared to that of the nanocomposite reinforced with P-SWCNTs,  
7 indicating the effectiveness of biofunctionalization to facilitate load transfer. The  
8 nanocomposite high strength provided by the biomolecules interactions make these  
9 multifunctional nanocomposites a good choice for the fabrication of high-performance  
10 nanocomposite-based devices in micro electromechanical systems and microelectronics.  
11 Considering the ability to change the electrical conductivity of the microfibers under mechanical  
12 disturbances and also by capturing biomolecules, the utilization of these multifunctional  
13 nanocomposite materials enables the fabrication of easily-manipulated strain sensors and porous  
14 microfibers or 3D complex patterns as solid support materials for potential biosensor  
15 applications.

16

## 17 **Acknowledgements**

18 The authors acknowledge the financial support from FQRNT (Le Fonds Québécois de la  
19 Recherche sur la Nature et les Technologies). Prof. El Khakani acknowledges also the financial  
20 support from NSERC (National Science Engineering Research Council of Canada) and Plasma-  
21 Québec (le Réseau Stratégique du FQRNT sur la Science et Technologies des Plasmas). The  
22 authors would like to thank the technical support of Dr. K. Laaziri from Laboratoire de  
23 recherche sur les nanostructures et interfaces conductrices for the electrical measurements.

24

## 25 **References**

- 1 [1] Dharap P, Li ZL, Nagarajaiah S, Barrera EV. Nanotube film based on single-wall carbon  
2 nanotubes for strain sensing. *Nanotechnology*. 2004;15(3):379-382.
- 3 [2] Su PG, Huang SC. Electrical and humidity sensing properties of carbon nanotubes-SiO<sub>2</sub>-poly (2-  
4 acrylamido-2-methylpropane sulfonate) composite material. *Sensors and Actuators B-Chemical*.  
5 2006;113(1):142-149.
- 6 [3] Qian D, Wagner GJ, Liu WK, Yu M-F, Ruoff RS. *Applied Mechanical Review*. 2002;55(6):495-  
7 532.
- 8 [4] Tans SJ, Devoret MH, Dai HJ, Thess A, Smalley RE, Geerligs LJ, et al. Individual single-wall  
9 carbon nanotubes as quantum wires. *Nature*. 1997;386(6624):474-477.
- 10 [5] Coleman JN, Khan U, Gun'ko YK. Mechanical reinforcement of polymers using carbon  
11 nanotubes. *Advanced Materials*. 2006;18(6):689-706.
- 12 [6] Ear Y, Silverman E. Challenges and opportunities in multifunctional nanocomposite structures  
13 for aerospace applications. *MRS Bulletin*. 2007;32(4):328-334.
- 14 [7] Mirfakhrai T, Krishna-Prasad R, Nojeh A, Madden JDW. Electromechanical actuation of single-  
15 walled carbon nanotubes: an ab initio study. *Nanotechnology*. 2008;19(31):1-8.
- 16 [8] Sahoo NG, Jung YC, Yoo HJ, Cho JW. Influence of carbon nanotubes and polypyrrole on the  
17 thermal, mechanical and electroactive shape-memory properties of polyurethane nanocomposites.  
18 *Composites Science and Technology*. 2007;67(9):1920-1929.
- 19 [9] Zhu J, Peng HQ, Rodriguez-Macias F, Margrave JL, Khabashesku VN, Imam AM, et al.  
20 Reinforcing epoxy polymer composites through covalent integration of functionalized nanotubes.  
21 *Advanced Functional Materials*. 2004;14(7):643-648.
- 22 [10] Atashbar MZ, Bejcek B, Singamaneni S, Santucci S. Carbon nanotube based biosensors.  
23 *Proceedings of the IEEE Sensors 2004*, 1-3:1048-1051.
- 24 [11] Kong J, Franklin NR, Zhou CW, Chapline MG, Peng S, Cho KJ, et al. Nanotube molecular  
25 wires as chemical sensors. *Science*. 2000;287(5453):622-625.
- 26 [12] Sun L, Warren GL, O'Reilly JY, Everett WN, Lee SM, Davis D, et al. Mechanical properties of  
27 surface-functionalized SWCNT/epoxy composites. *Carbon*. 2008;46(2):320-328.
- 28 [13] Wang S, Liang R, Wang B, Zhang C. Reinforcing polymer composites with epoxide-grafted  
29 carbon nanotubes. *Nanotechnology*. 2008;19(8):1-7.
- 30 [14] Wang SR, Liang ZY, Liu T, Wang B, Zhang C. Effective amino-functionalization of carbon  
31 nanotubes for reinforcing epoxy polymer composites. *Nanotechnology*. 2006;17(6):1551-1557.
- 32 [15] Zhao JX, Ding YH. Functionalization of single-walled carbon nanotubes with metalloporphyrin  
33 complexes: A theoretical study. *Journal of Physical Chemistry C*. 2008;112(30):11130-11134.
- 34 [16] Zhu J, Kim JD, Peng HQ, Margrave JL, Khabashesku VN, Barrera EV. Improving the  
35 dispersion and integration of single-walled carbon nanotubes in epoxy composites through  
36 functionalization. *Nano Letters*. 2003;3(8):1107-1113.
- 37 [17] Chen J, Hamon MA, Hu H, Chen YS, Rao AM, Eklund PC, et al. Solution properties of single-  
38 walled carbon nanotubes. *Science*. 1998;282(5386):95-98.
- 39 [18] Nakashima N, Fujigaya T. Fundamentals and applications of soluble carbon nanotubes.  
40 *Chemistry Letters*. 2007;36(6):692-697.
- 41 [19] Holmberg A, Blomstergren A, Nord O, Lukacs M, Lundeberg J, Uhlen M. The biotin-  
42 streptavidin interaction can be reversibly broken using water at elevated temperatures.  
43 *Electrophoresis*. 2005;26(3):501-510.
- 44 [20] Laitinen OH, Hytonen VP, Nordlund HR, Kulomaa MS. Genetically engineered avidins and  
45 streptavidins. *Cellular and Molecular Life Sciences*. 2006;63(24):2992-3017.
- 46 [21] Patel AC, Li SX, Yuan JM, Wei Y. In situ encapsulation of horseradish peroxidase in  
47 electrospun porous silica fibers for potential biosensor applications. *Nano Letters*. 2006;6(5):1042-  
48 1046.

- 1 [22] Lebel LL, Aissa B, El Khakani MA, Therriault D. Preparation and mechanical characterization  
2 of laser ablated single-walled carbon-nanotubes/polyurethane nanocomposite microbeams.  
3 Composites Science and Technology. 2010;70(3):518-524.
- 4 [23] Lebel LL, Aissa B, El Khakani MA, Therriault D. Ultraviolet-Assisted Direct-Write  
5 Fabrication of Carbon Nanotube/Polymer Nanocomposite Microcoils. Advanced Materials.  
6 2010;22(5):592-596.
- 7 [24] Braidy N, El Khakani MA, Botton GA. Effect of laser intensity on yield and physical  
8 characteristics of single wall carbon nanotubes produced by the Nd : YAG laser vaporization  
9 method. Carbon. 2002;40(15):2835-2842.
- 10 [25] Le Borgne V, Aissa B, Mohamedi M, Kim YA, Endo M, El Khakani MA. Pulsed KrF-laser  
11 synthesis of single-wall-carbon-nanotubes: effects of catalyst content and furnace temperature on  
12 their nanostructure and photoluminescence properties, 2011;13 (11):5759-5768.
- 13 [26] Thostenson ET, Chou TW. Processing-structure-multi-functional property relationship in  
14 carbon nanotube/epoxy composites. Carbon. 2006;44(14):3022-3029.
- 15 [27] Therriault D, Shepherd RF, White SR, Lewis JA. Fugitive inks for direct-write assembly of  
16 three-dimensional microvascular networks. Advanced Materials. 2005;17(4):395-399.
- 17 [28] Bachilo SM, Strano MS, Kittrell C, Hauge RH, Smalley RE, Weisman RB. Structure-assigned  
18 optical spectra of single-walled carbon nanotubes. Science. 2002;298(5602):2361-2366.
- 19 [29] Okpalugo TIT, Papakonstantinou P, Murphy H, McLaughlin J, Brown NMD. High resolution  
20 XPS characterization of chemical functionalised MWCNTs and SWCNTs. Carbon. 2005;43(1):153-  
21 161.
- 22 [30] Bruneaux J, Therriault D, Heuzey MC. Micro-extrusion of organic inks for direct-write  
23 assembly. Journal of Micromechanics and Microengineering. 2008;18(11):1-8
- 24 [31] Wang D, Sun G, Xiang B, Chiou BS. Controllable biotinylated polyethylene-co-glycidyl  
25 methacrylate) (PE-co-GMA) nanofibers to bind streptavidin-horseradish peroxidase (HRP) for  
26 potential biosensor applications. European Polymer Journal. 2008;44(7):2032-2039.
- 27 [32] Moussaddy H, Farahani RD, El Khakani MA, Lévesque M, Therriault D. Mechanical  
28 properties of chemically-treated carbon nanotube nanocomposite microfibers: experimental and  
29 modeling studies. The second joint US-Canada conference on composites, 2011.
- 30 [33] Winey KI, Kashiwagi T, Mu MF. Improving electrical conductivity and thermal properties of  
31 polymers by the addition of carbon nanotubes as fillers. Mrs Bulletin. 2007;32(4):348-353.
- 32 [34] Sotiropoulou S, Chaniotakis NA. Carbon nanotube array-based biosensor. Analytical and  
33 Bioanalytical Chemistry. 2003;375(1):103-105.

## 36 **Figures and Tables captions**

37 **Figure 1.** Schematic representation of the UV-assisted direct-writing of nanocomposite  
38 microfibers: (a) nanocomposite extrusion through a capillary micronozzle by an applied pressure;  
39 fibers are partially cured shortly after extrusion under UV illumination, (b) close-up view of the  
40 microfibers, and (c) interfacial bonding between SWCNTs and epoxy matrix through biotin-  
41 streptavidin interactions.

1 **Figure 2.** (a) Raman spectra, (b) X-ray photoelectron spectra of as-produced (bottom) and purified  
2 (top) SWCNTs, (c) typical TEM image of as-produced SWCNTs, and (d) TEM image of P-  
3 SWCNTs.

4 **Figure 3.** (a) FT-IR spectra of (i) P-SWCNTs (bottom), (ii) aminated SWCNTs (middle), and (iii)  
5 biotinylated SWCNTs (BF-SWCNTs) (top), (b) high-resolution TEM image of a P-SWCNTs, and  
6 (c) high-resolution TEM image of a BF-SWCNTs.

7

8 **Figure 4.** Optical microscope images of a 20- $\mu$ m thick film of the nanocomposite containing (a) 1  
9 wt% P-SWCNTs and (b) 1 wt% BF-SWCNTs, (c) and (d) typical SEM images of the cross-section  
10 surface of the bulk nanocomposites containing 1 wt% P-SWCNTs and 1 wt% BF-SWCNTs,  
11 respectively.

12

13 **Figure 5.** Mechanical characterization of the nanocomposite materials: (a) optical image of a  
14 typical fabricated specimen consisting of three suspended fibers between two rectangular pads, (b)  
15 SEM image of fracture surface of a nanocomposite fiber, (c) typical stress–strain curves and (d)  
16 histograms of modulus, strength and failure strain of the pure UV-epoxy and its associated  
17 nanocomposites.

18

19 **Figure 6.** Schematics of (a) synthesis procedure of the BF-SWCNTs and (b) proposed interaction  
20 mechanisms governing the interaction of the BF-SWCNTs and the epoxy matrix by bridge formation  
21 through biotin-streptavidin interactions.

22

23 **Figure 7.** Measured current upon voltage application for the nanocomposite microfibers.

24

25

26

1 **Table 1.** Comparison of the mechanical properties improvements in our work with those reported in  
2 literature.

3

4 **Table 1**

SWCNTs type	SWCNTs wt. %	Processing method	Modulus (% increase)	Strength (% increase)	Ref.
NH <sub>2</sub> -modified	1.0	Solution mixing	31	25	[9]
Amine-modified	1.0	Simple mixing	26	16	[12]
Epoxide-modified	1.0	Solution mixing	60	40	[13]
Carboxyl-modified	1.0	Shear mixing	24	-	[?]
NH <sub>2</sub> -modified	0.1	Simple mixing	56	12	[?]
Fluorinated	1.0	Solution mixing	30	18	[?]
Purified	5.0	Solution mixing	0	7	[?]
Bio-functionalized	1.0	Solution & shear mixing	93	75	Present work

5

6

**Figure 1**

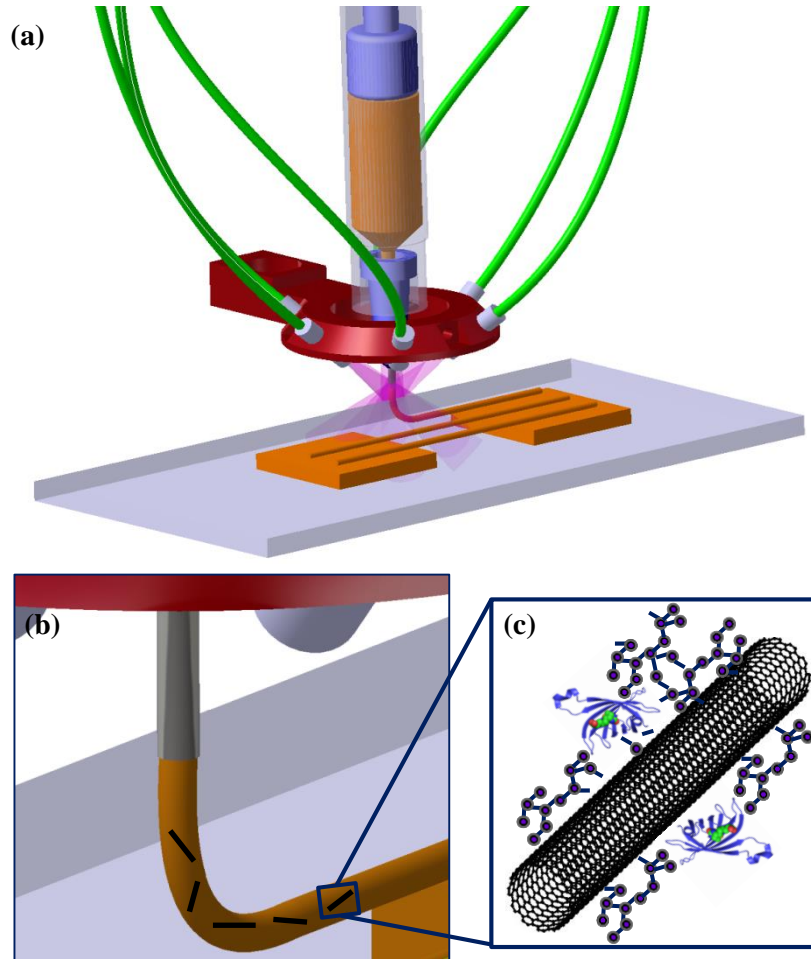


**Figure 2**

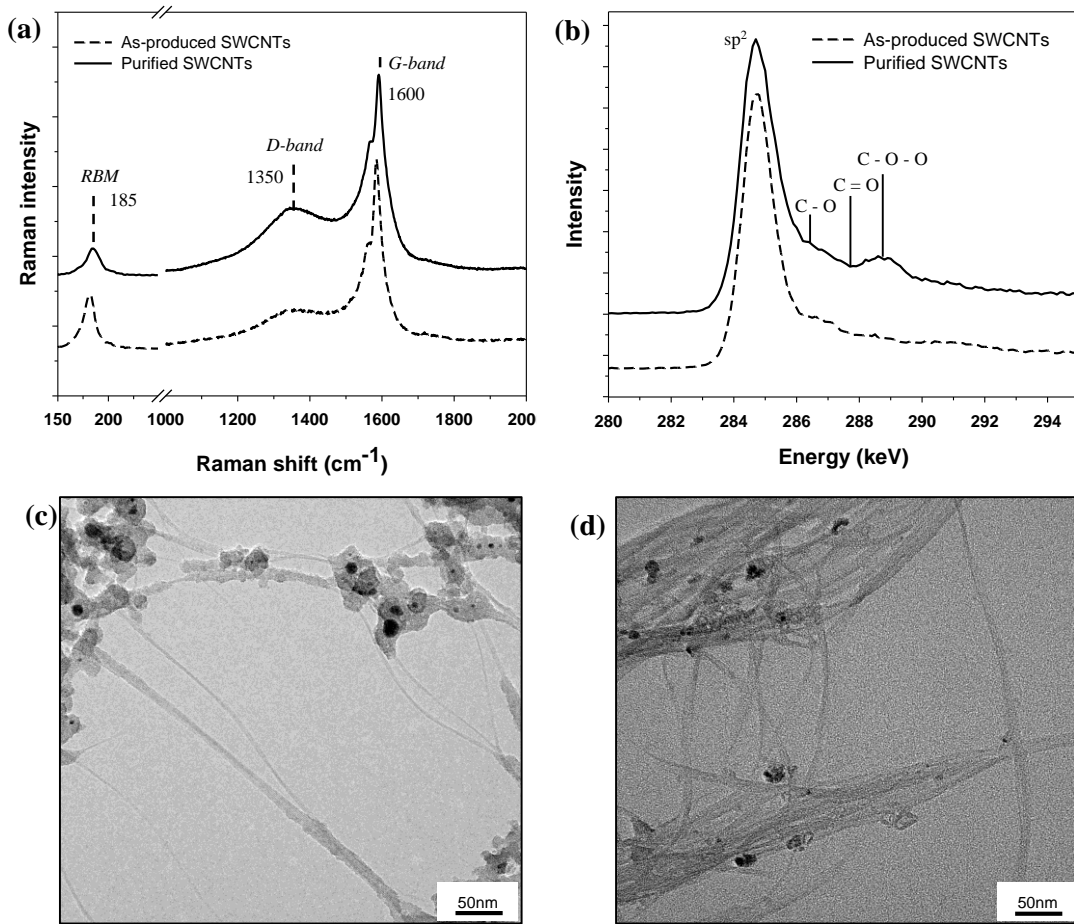


**Figure 3**

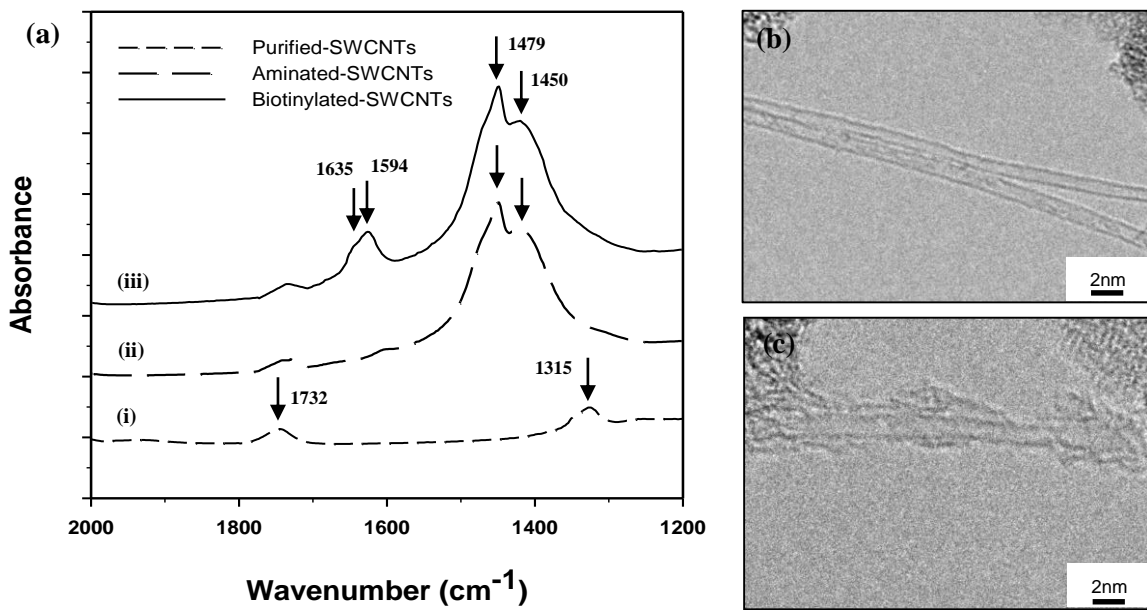


**Figure 4**

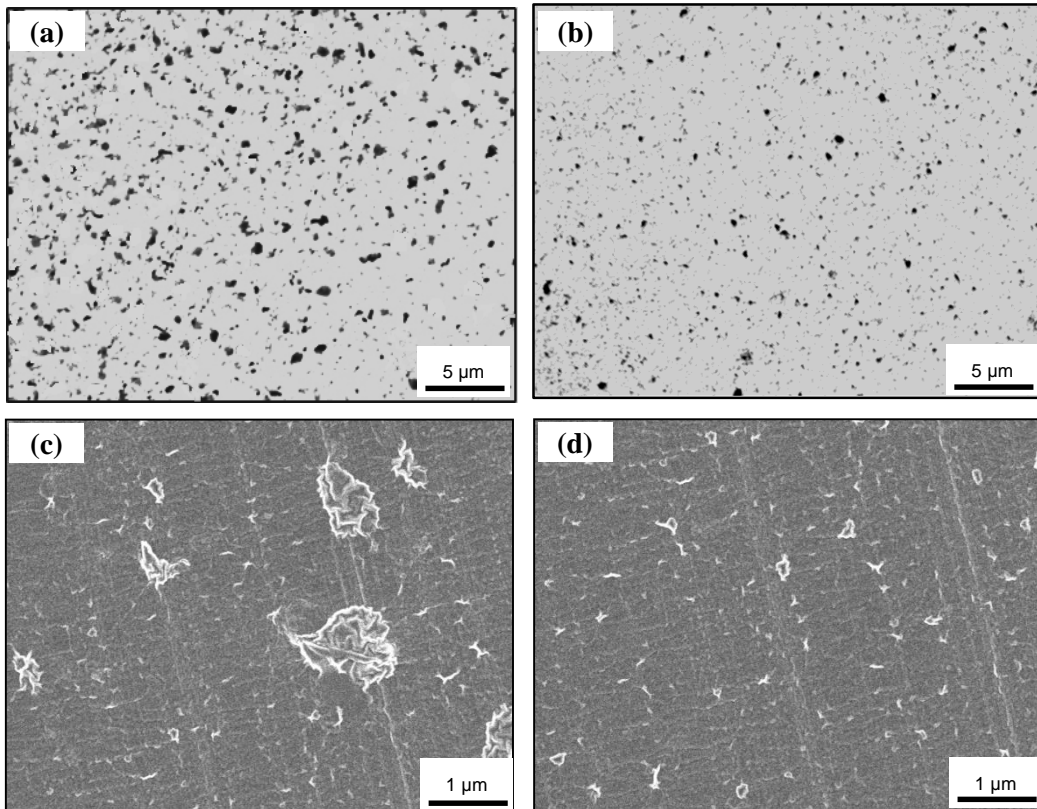


**Figure 5**

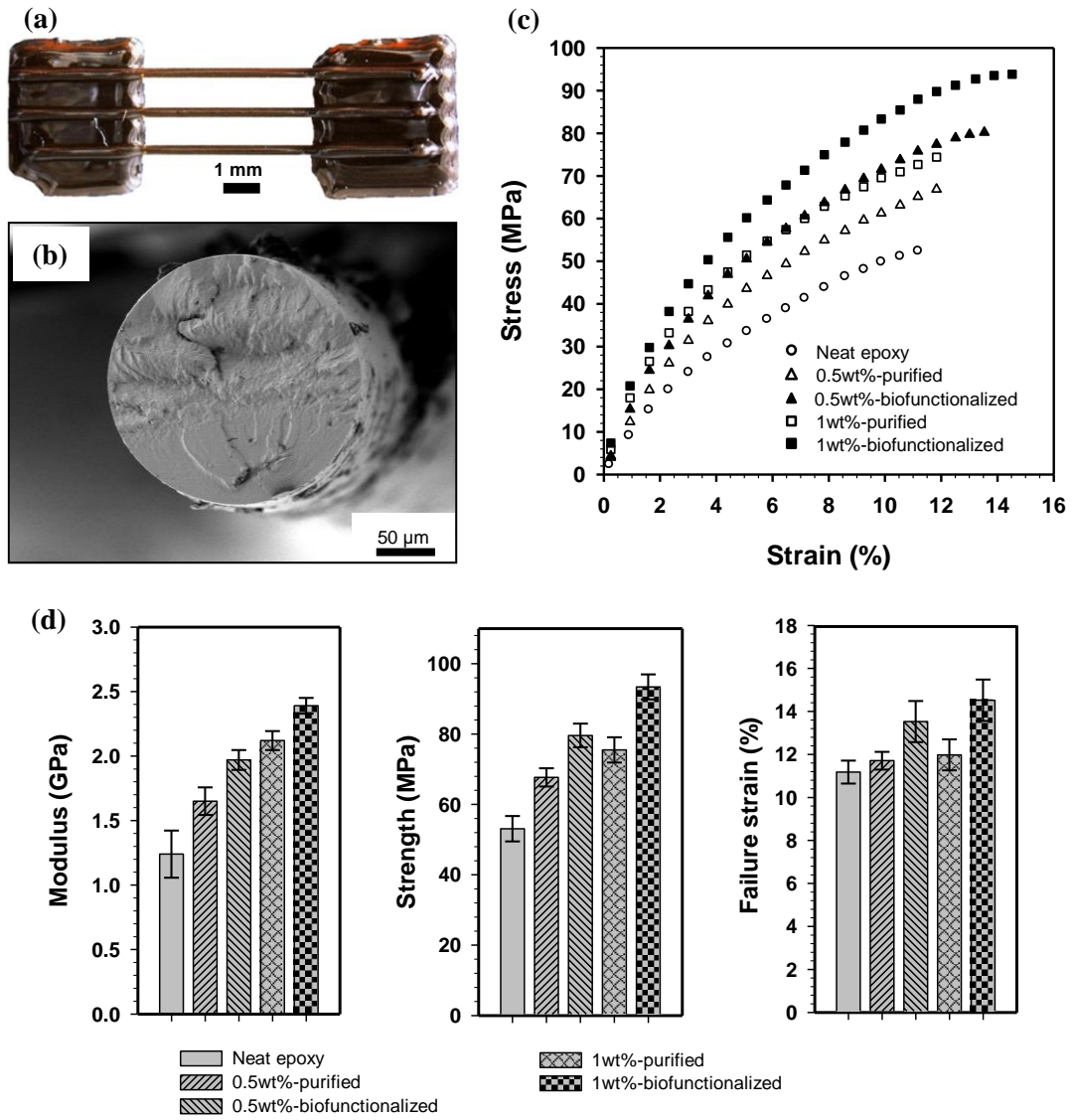


# Figure 6

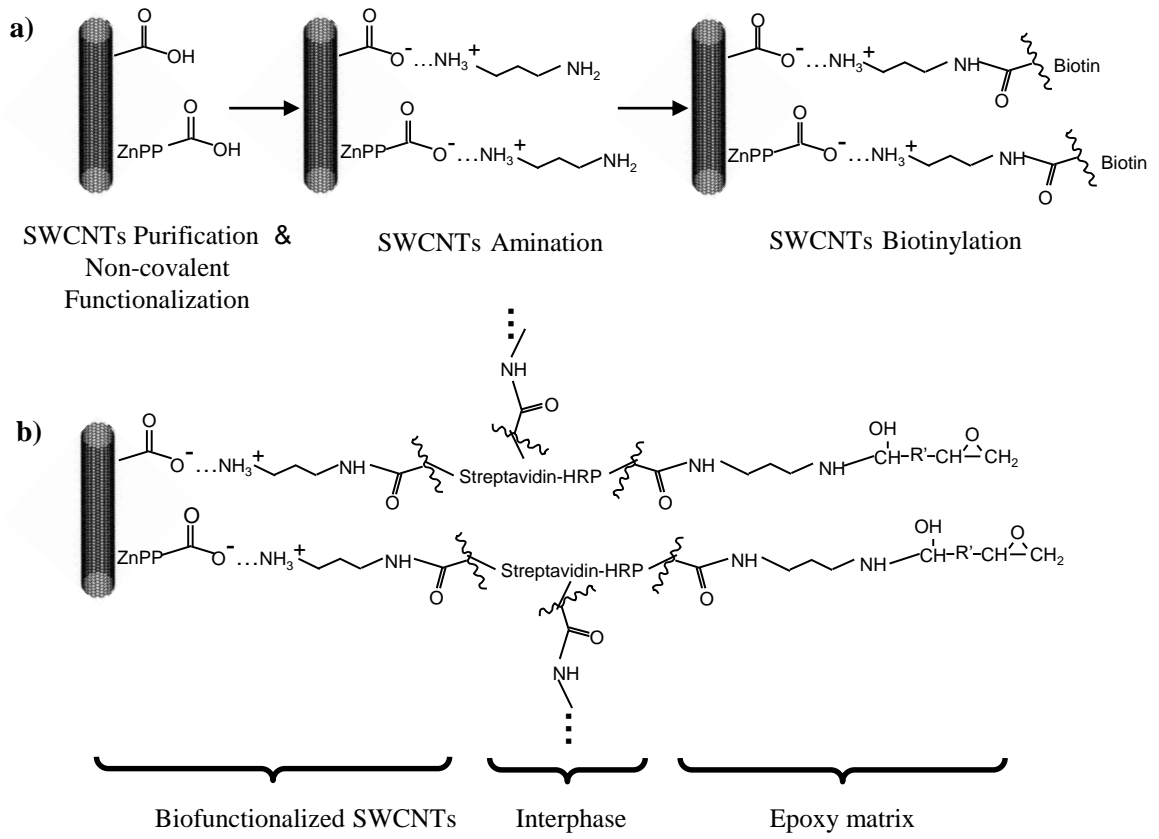


# Figure 7

